Room Temperature Quantum Coherence and Rabi Oscillations in Vanadyl Phthalocyanine: Toward Multifunctional Molecular Spin Qubits

Matteo Atzori,[†] Lorenzo Tesi,[†] Elena Morra,[†] Mario Chiesa,[†] Lorenzo Sorace,[†] and Roberta Sessoli*[,†]

† Dipartimento di Chimica "Ugo Schiff" & INSTM RU, Università degli Studi di Firenze, Via della Lastruccia 3, I50019 Sesto Fiorentino (Firenze), Italy.

‡ Dipartimento di Chimica & NIS Centre, Università di Torino, Via P. Giuria 7, I10125 Torino, Italy.

SUPPORTING INFORMATION

Crystal Structure

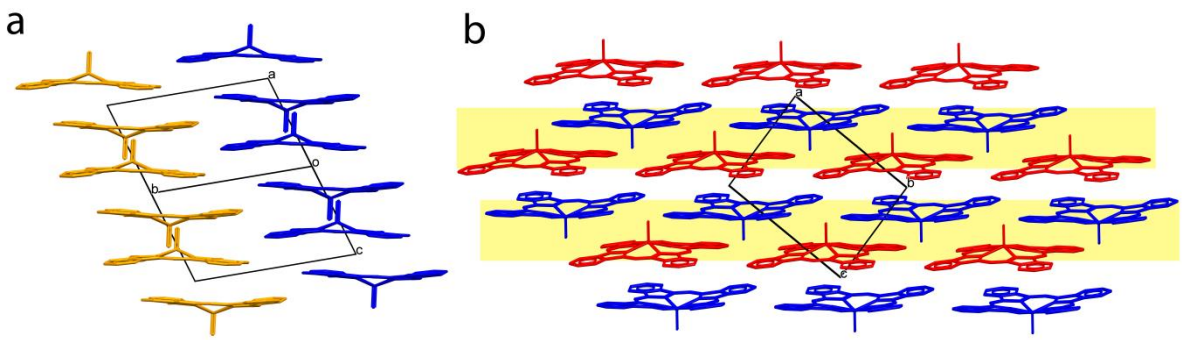

Figure S1. (a) View of the crystal structure of **1** where the stacked VOPc molecules are highlighted. (b) View of the molecular disposition of the VOPc molecules inside each layer parallel to the *ac* plane, and collinear orientation of the VO moieties.

Powder X-ray Crystallography

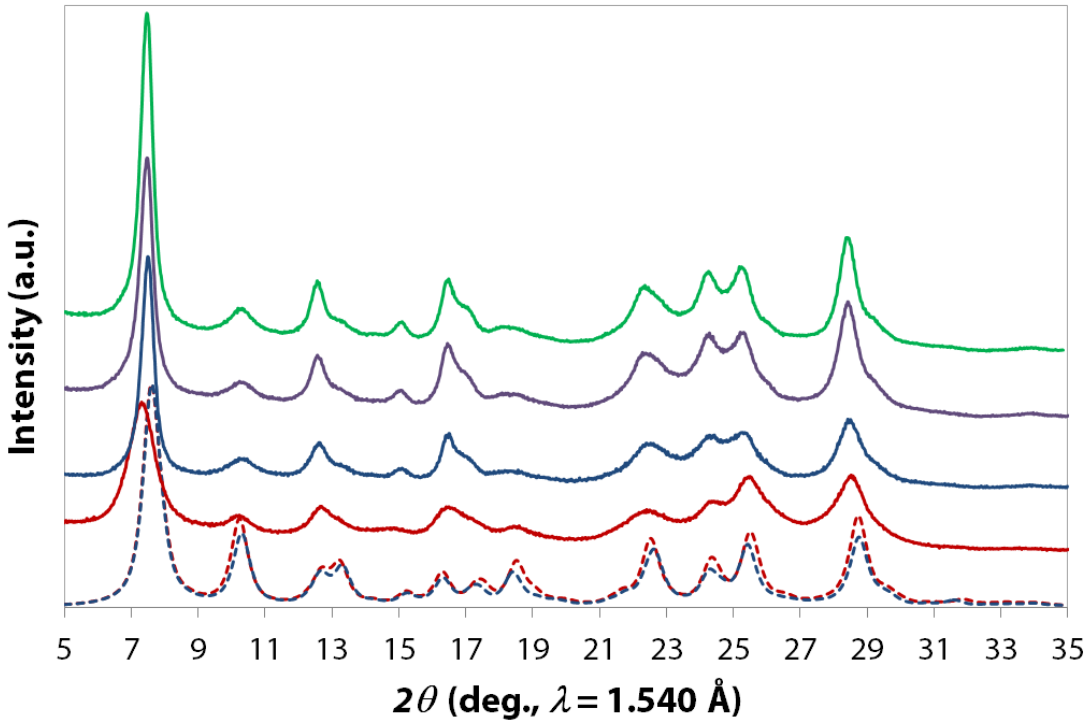

Figure S2. Comparison between experimental (solid lines) and simulated (dashed lines) PXRD patterns (5–35°, *2θ*) for TiOPc-II (blue line), VOPc-II (**1**) (red line), VOPc:TiOPc$_{1:10}$-II (**2**) (violet line), and VOPc:TiOPc$_{1:1000}$-II (**3**) (green line).

AC Susceptometry

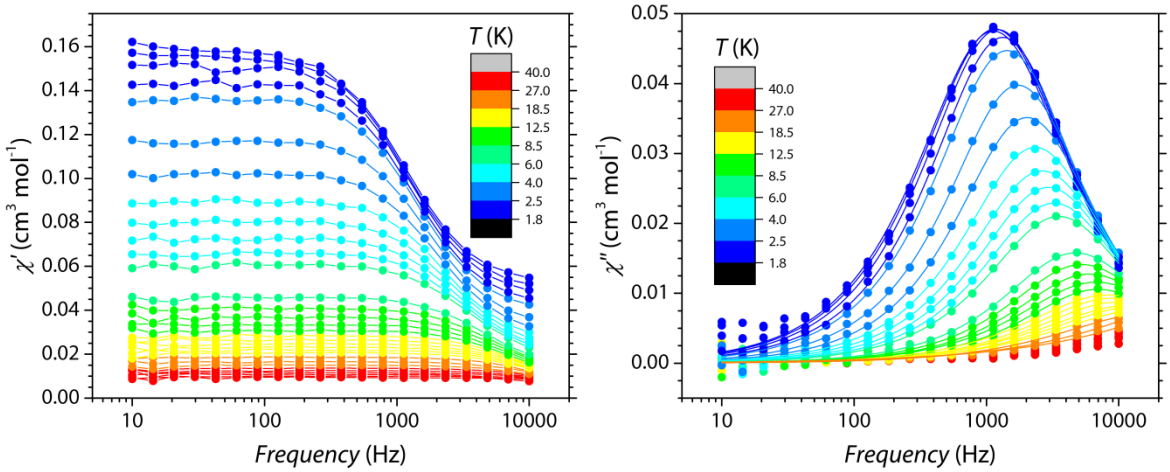

Figure S3. Frequency dependence of the real component χ' (left) and the imaginary component χ'' (right) of the magnetic susceptibility of **1** as a function of the temperature (1.8–40 K range) under an applied static magnetic field of 0.2 T.

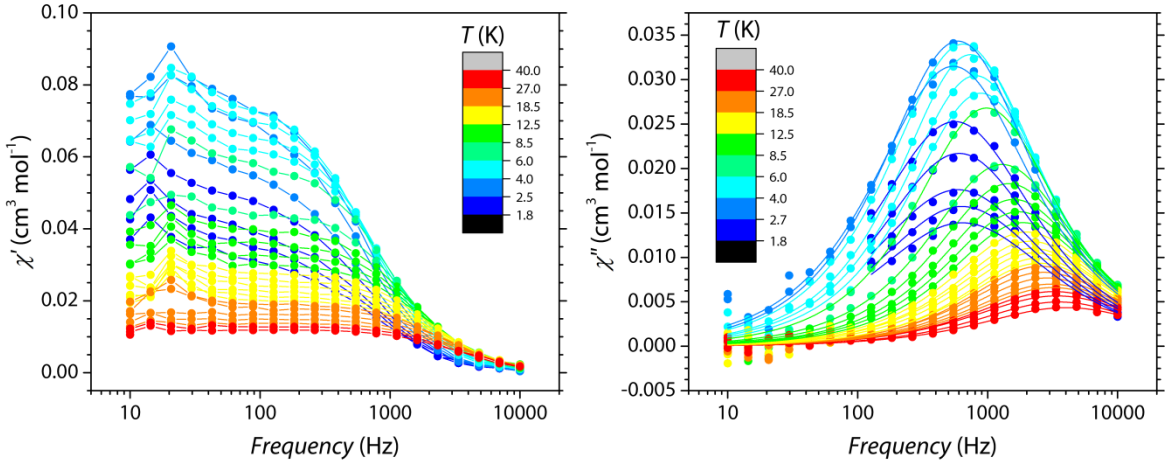

Figure S4. Frequency dependence of the real component χ' (left) and the imaginary component χ'' (right) of the magnetic susceptibility of **1** as a function of the temperature (1.8–40 K range) under an applied static magnetic field of 1.0 T.

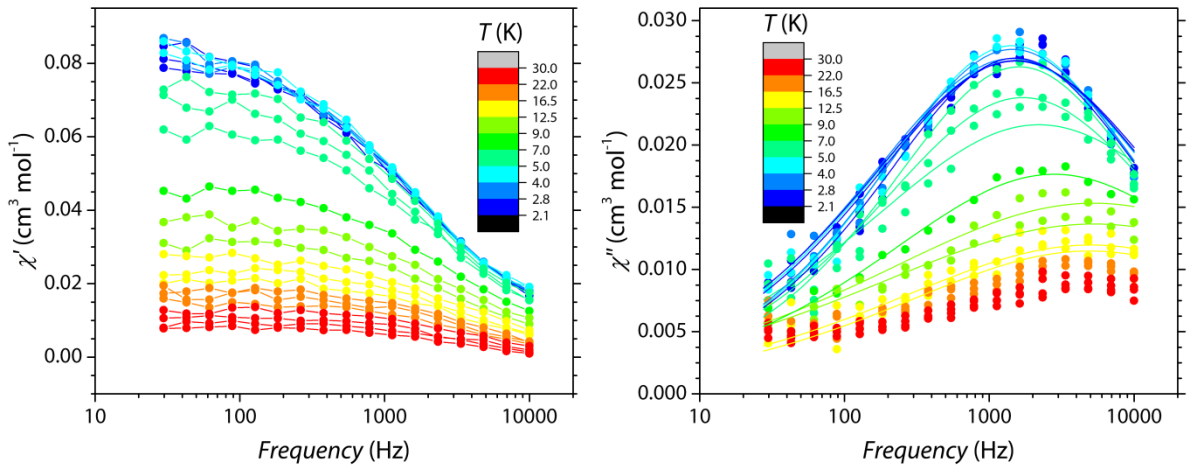

Figure S5. Frequency dependence of the real component χ' (left) and the imaginary component χ'' (right) of the magnetic susceptibility of **2** as a function of the temperature (2.1–30 K range) under an applied static magnetic field of 0.2 T.

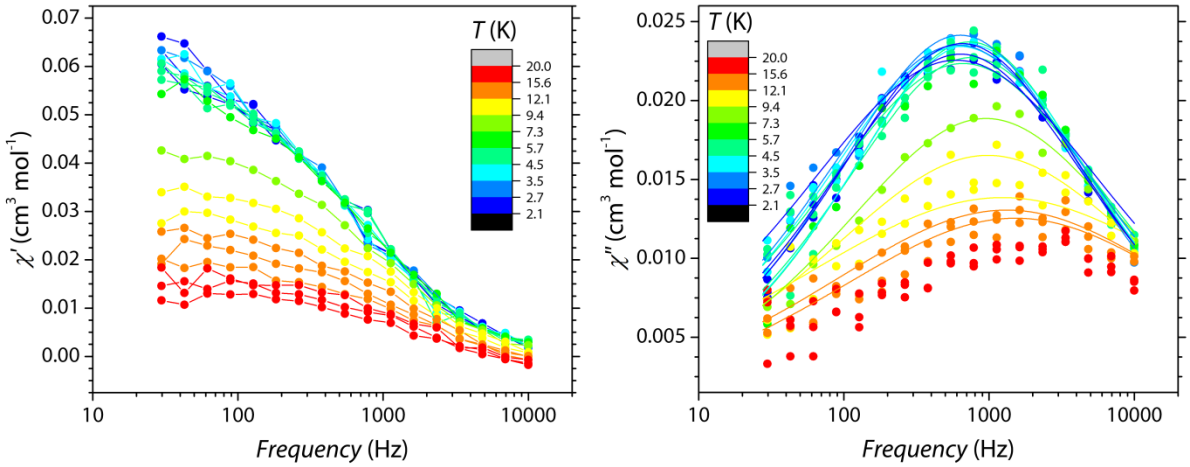

Figure S6. Frequency dependence of the real component χ' (left) and the imaginary component χ'' (right) of the magnetic susceptibility of **2** as a function of the temperature (2.1–20 K range) under an applied static magnetic field of 1.0 T.

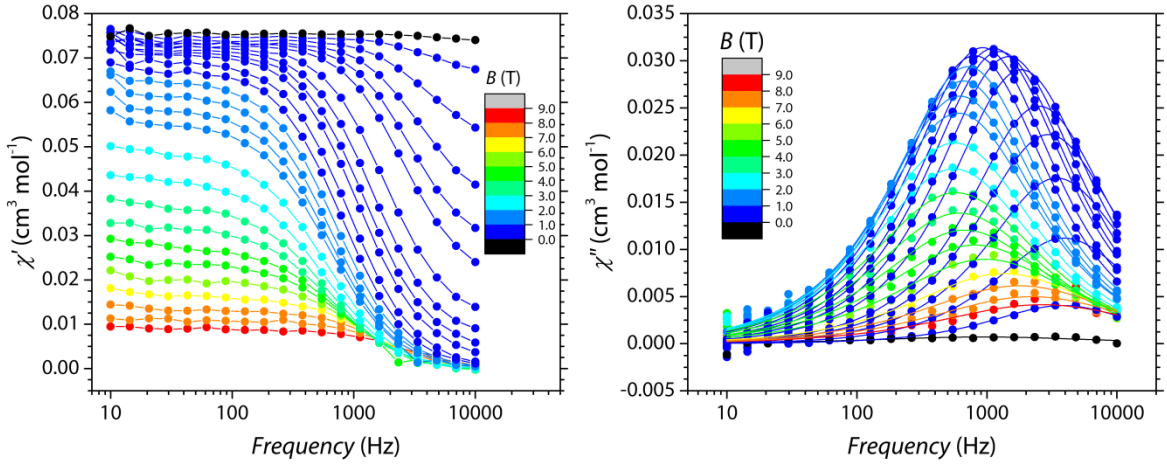

Figure S7. Frequency dependence of the real component χ' (left) and the imaginary component χ'' (right) of the magnetic susceptibility of **1** as a function of the magnetic field (0.0–8.8 T range) at T = 5 K.

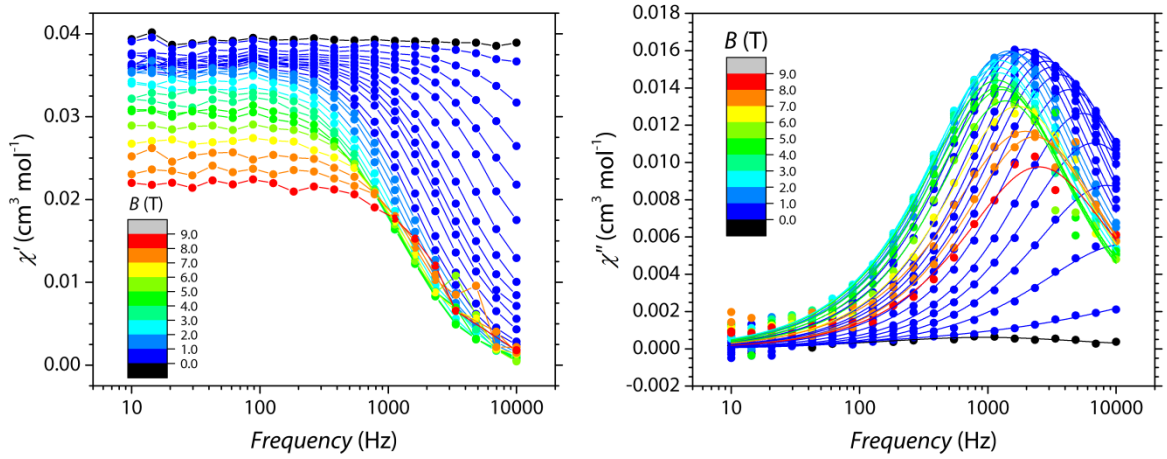

Figure S8. Frequency dependence of the real component χ' (left) and the imaginary component χ'' (right) of the magnetic susceptibility of **1** as a function of the magnetic field (0.0–8.8 T range) at T = 10 K.

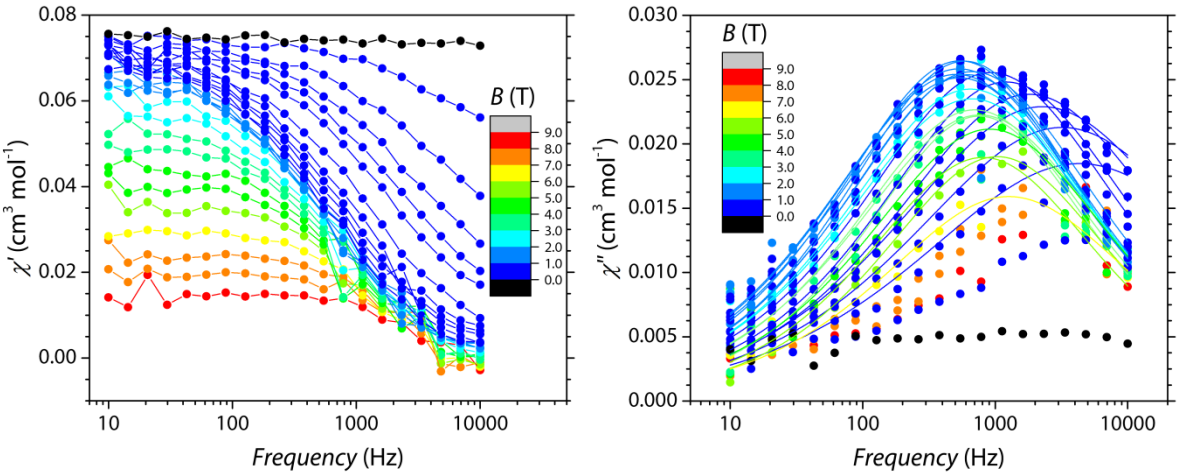

Figure S9. Frequency dependence of the real component χ' (left) and the imaginary component χ'' (right) of the magnetic susceptibility of **2** as a function of the magnetic field (0.0–8.8 T range) at T = 5 K.

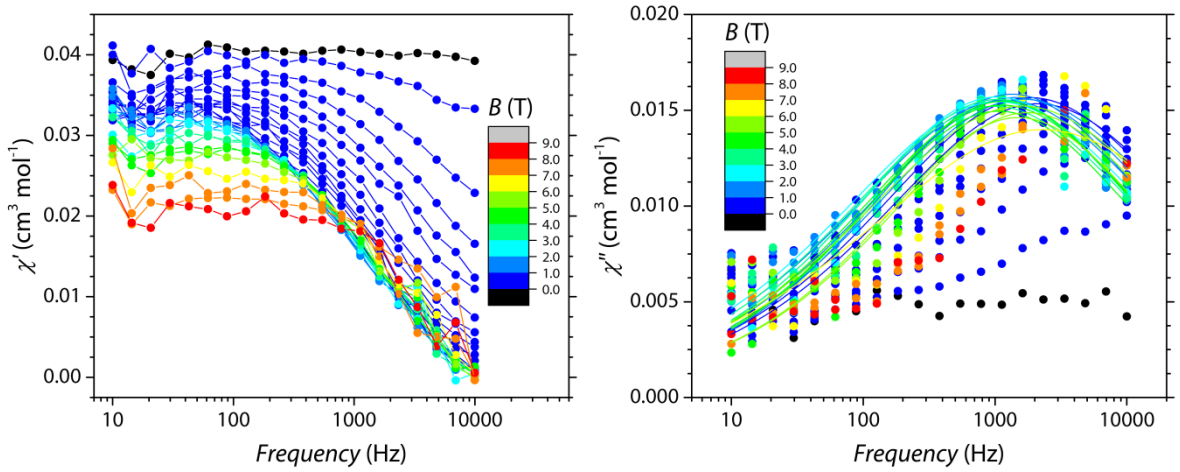

Figure S10. Frequency dependence of the real component χ' (left) and the imaginary component χ'' (right) of the magnetic susceptibility of **2** as a function of the magnetic field (0.0–8.8 T range) at T = 10 K.

Table S1. Best-fit parameters of the model (Equation 1, main text) used to reproduce the field dependence of the magnetization relaxation rate for **1** and **2** at T = 5 K and 10 K.

Compound	T (K)	c ($T^{-4}ms^{-1}$)	d (ms^{-1})	e (ms^{-1})	f (ms^{-1})
1	5	0.0025(3)	18(1)	0.18(1)	0.71(6)
	10	0.0015(3)	45(4)	0.17(1)	0.48(5)
2	5	0.0032(4)	61(20)	0.06(4)	0.11(2)
	10	0.0086(8)	83(6)	0.07(1)	0.16(2)

CW-EPR Spectroscopy

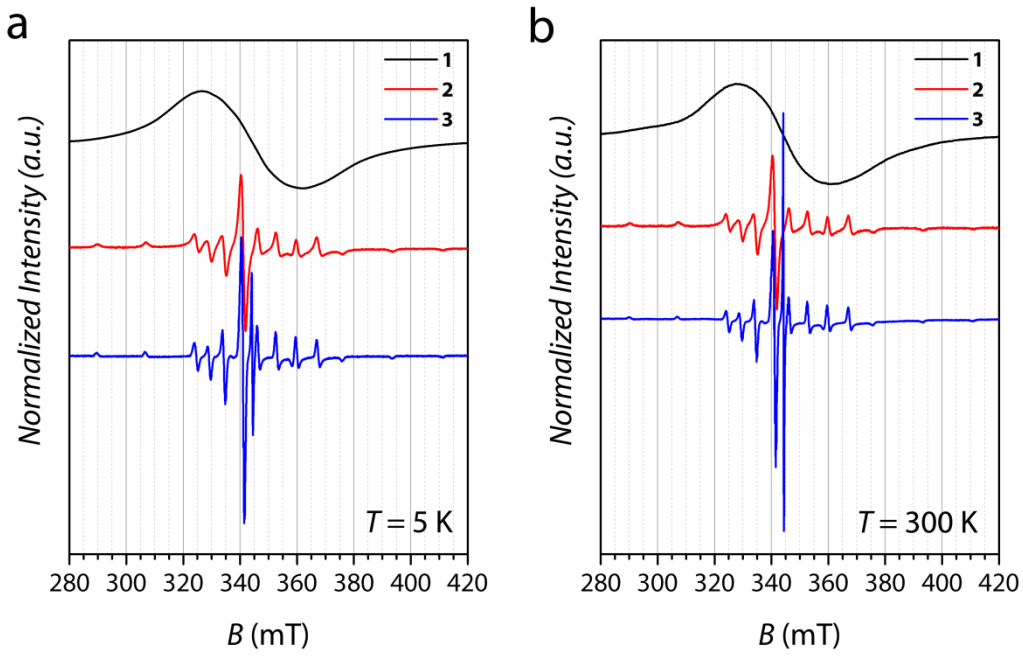

Figure S11. Experimental CW-EPR X-band spectra (9.47 GHz) for **1** (black line), **2** (red line) and **3** (blue line) at T = 5 K (a) and 300 K (b).

Table S2. Best-fit parameters of the model (Equation 2, main text) used to reproduce the EPR spectra of **2** and **3** at T = 300 K.

Compound	$g_{x,y}$	g_z	$^{V}A_{x,y}$ (cm^{-1})	$^{V}A_z$ (cm^{-1})	$^{N}A_{iso}$ (cm^{-1})
2	1.989(1)	1.967(1)	0.0057(1)	0.0158(1)	-
3	1.987(1)	1.966(1)	0.0056(1)	0.0159(1)	0.00025(1)

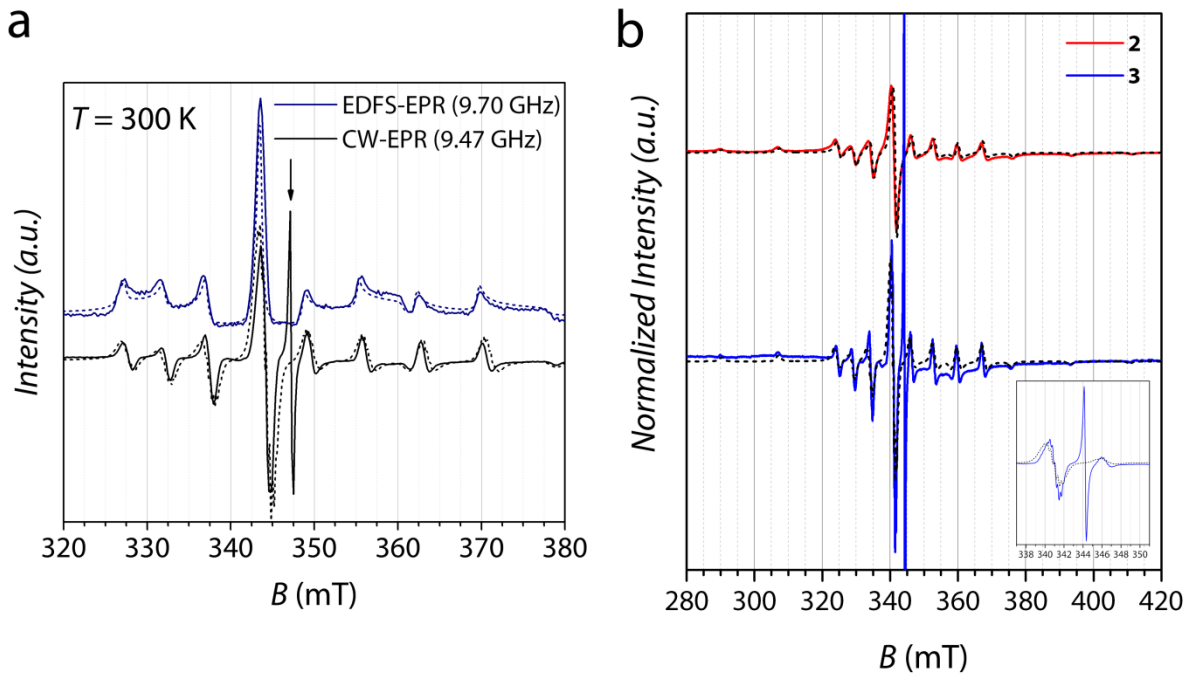

Figure S12. (a) Expanded view of the central portion of Figure 3a. (b) Experimental (solid lines) and simulated (black dotted lines) CW-EPR X-band spectra (9.47 GHz) for **2** (red line) and **3** (blue line) at T = 300 K. Inset shows in detail the signals of the so-called powder-like line of VOPc (left) and of the exchange-narrowed signal attributed to $TiOPc^{\cdot -}$ (right).

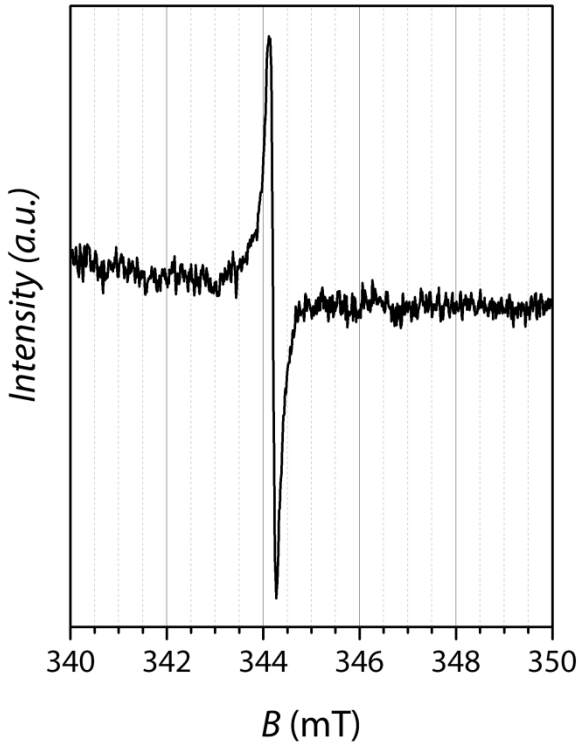

Figure S13. Experimental CW-EPR X-band spectra (9.47 GHz) of TiOPc-II as received from Sigma-Aldrich at T = 300 K.

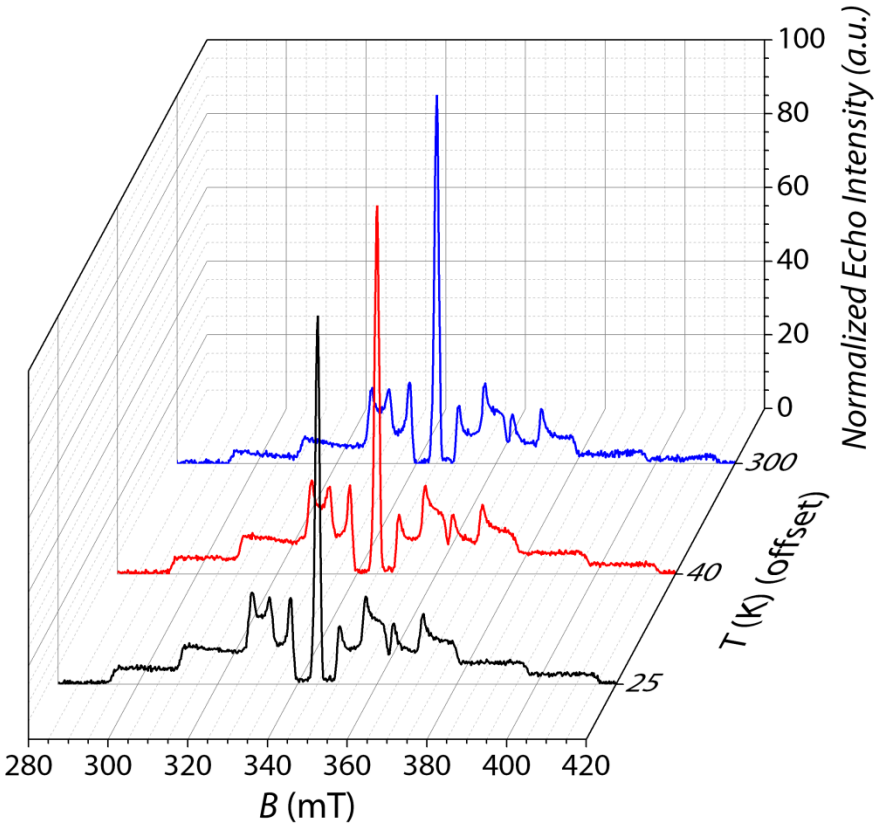

Figure S14. Normalized (0–100 a.u.) experimental EDFS-EPR X-band spectra (9.70 GHz) for **3** at different temperatures (offset).

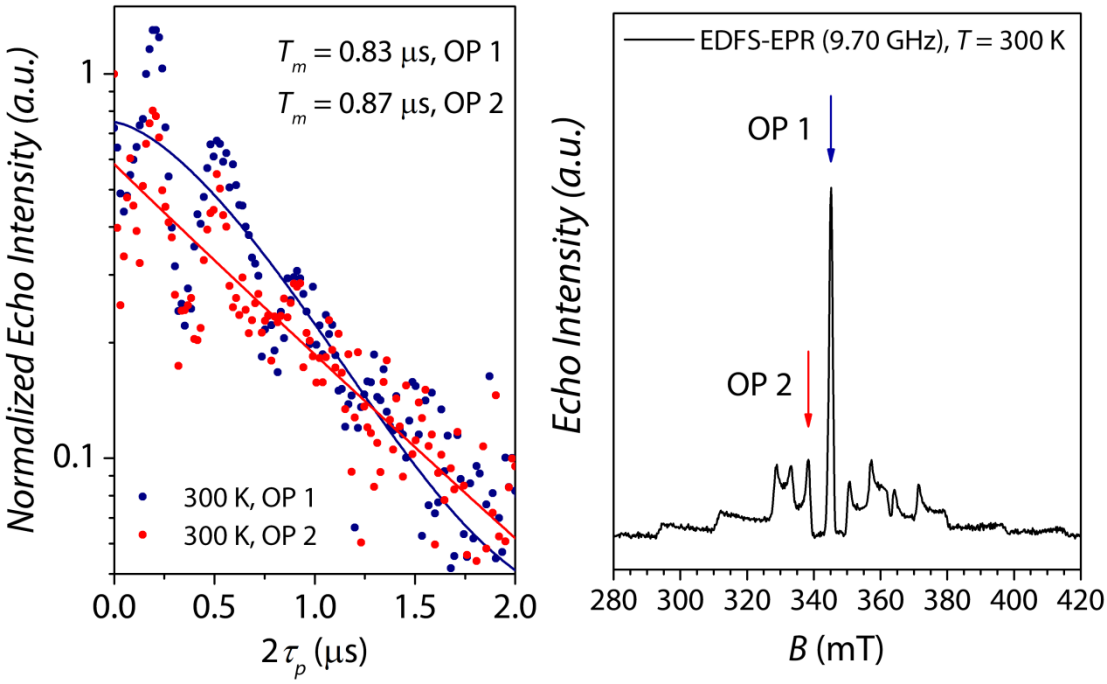

Figure S15. Echo decay traces for **3** (T = 300 K) at two different Observer Positions (OP).

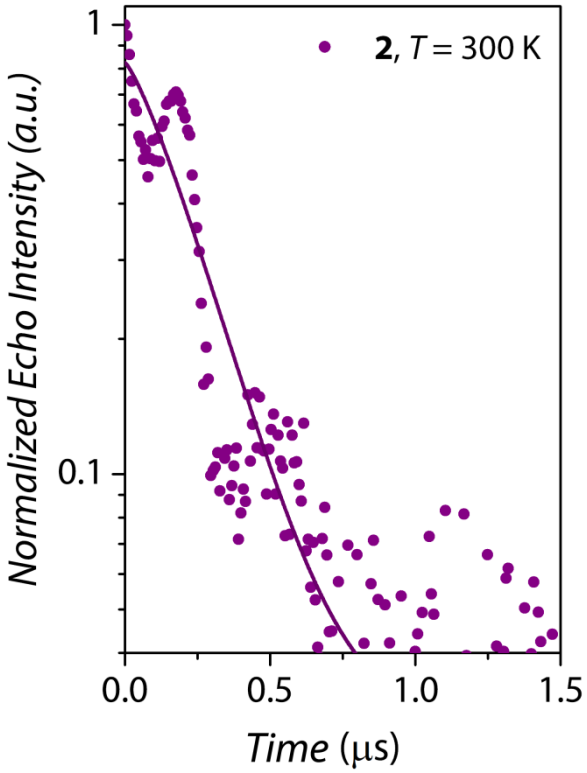

Figure S16. Echo decay trace for **2** T = 300 K.

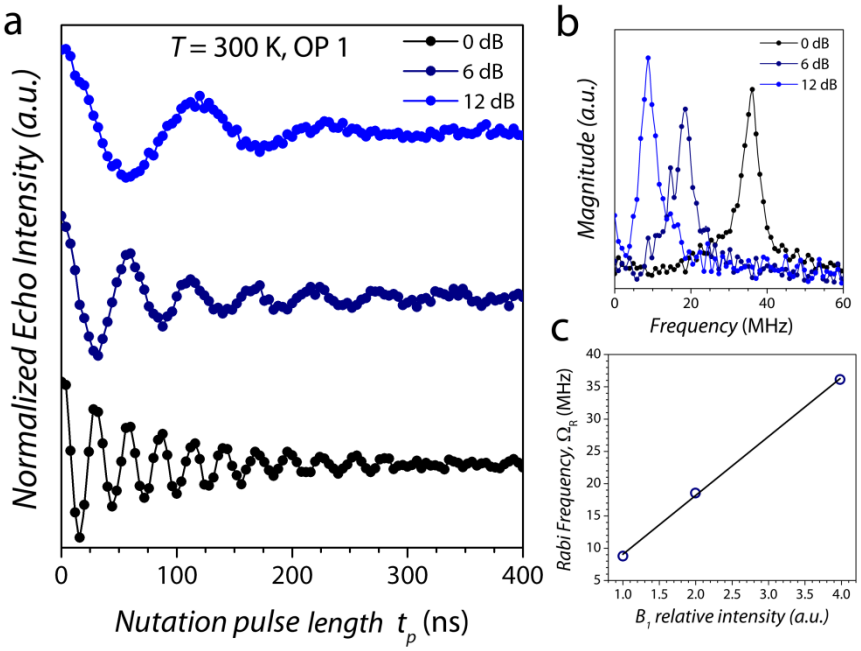

Figure S17. (a) Rabi oscillations for **3** recorded at 300 K (OP 1, see Figure S15) for different microwave attenuations. (b) Fourier Transform of the Rabi oscillations. (c) Linear dependence of the Rabi frequency (Ω_R) as a function of the relative intensity of the oscillating field B_1.

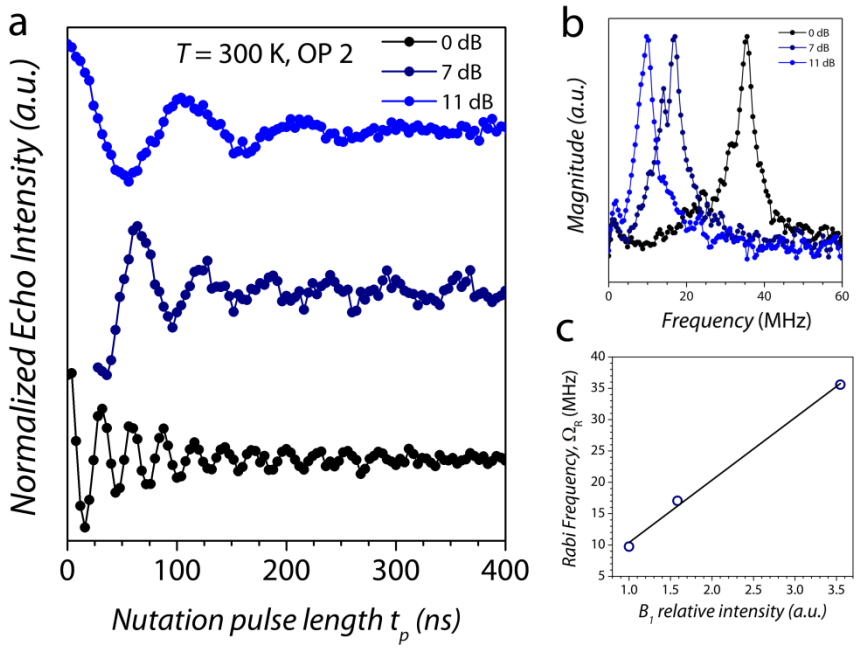

Figure S18. (a) Rabi oscillations for **3** recorded at 300 K (OP 2, see Figure S15) for different microwave attenuations. (b) Fourier Transform of the Rabi oscillations. (c) Linear dependence of the Rabi frequency (Ω_R) as a function of the relative intensity of the oscillating field B_1.

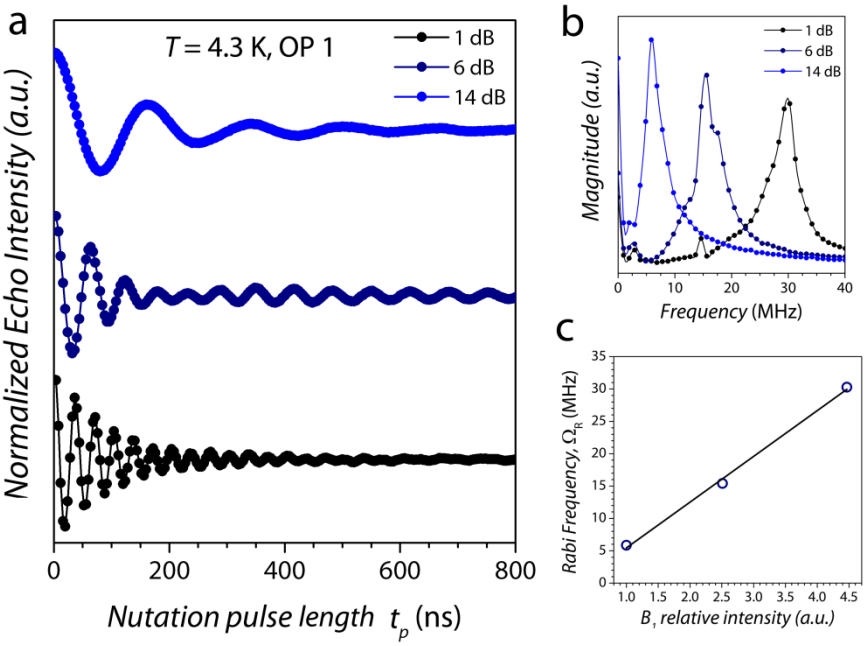

Figure S19. (a) Rabi oscillations for **3** recorded at 4.3 K (OP 1, see Figure S15) for different microwave attenuations. (b) Fourier Transform of the Rabi oscillations. (c) Linear dependence of the Rabi frequency (Ω_R) as a function of the relative intensity of the oscillating field B_1.

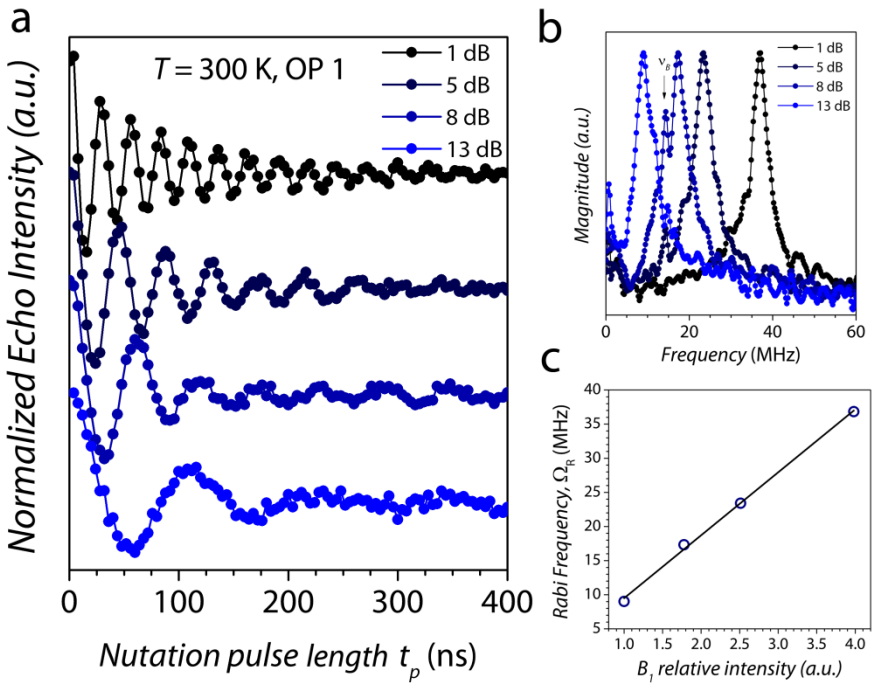

Figure S20. (a) Rabi oscillations for **2** recorded at 300 K (OP 1, see Figure S15) for different microwave attenuations. (b) Fourier Transform of the Rabi oscillations. (c) Linear dependence of the Rabi frequency (Ω_R) as a function of the relative intensity of the oscillating field B_1.

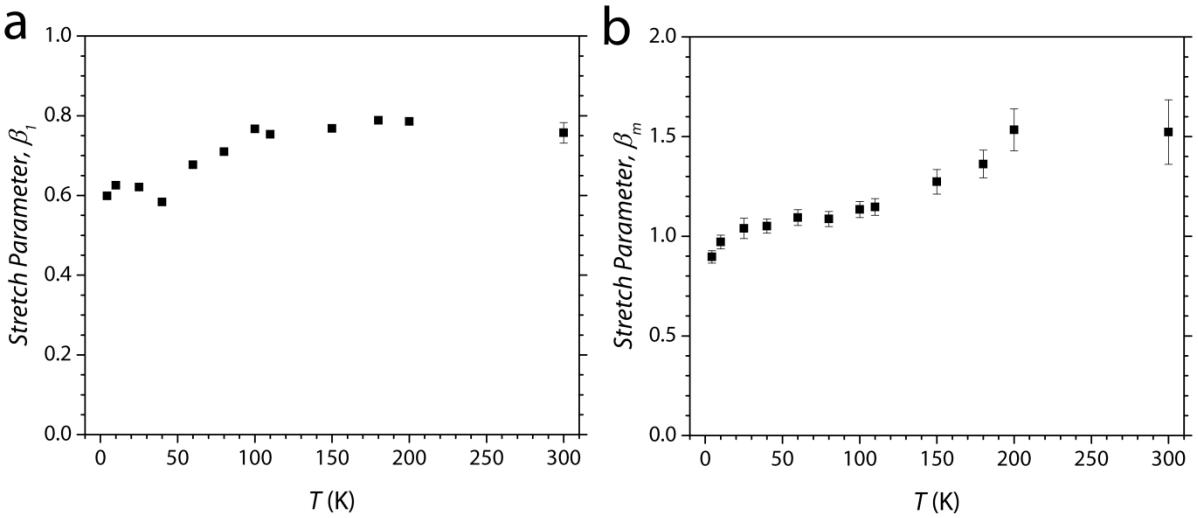

Figure S21. Temperature dependence of the best-fit values of the stretching parameters β_1 (a) and β_m (b) for **3**.

Equations

$$I = I_0 + k_1 exp\left[-\left(\frac{\tau}{T_1}\right)^{\beta_1}\right]$$

Equation S1. Stretched-exponential equation used for the fitting of the standard inversion recovery experiments. The temperature dependence of the best-fit values of the stretching parameter β_1 is reported in Figure S21a.

$$I = I_0 + k_m exp\left[-\left(\frac{2\tau}{T_m}\right)^{\beta m}\right]$$

Equation S2. Stretched-exponential equation used for the fitting of the echo decay traces reported in Figure 4a. The temperature dependence of the best-fit values of the stretching parameter β_m is reported in Figure S21b.

$$T_1{}^{-1} = aT + bT^n$$

Equation S3. Equation used for the fitting of the temperature dependence of the T_1^{-1} relaxation rate as a function of the temperature extracted from pulsed EPR experiments on 3. The best-fit values are a = 1.4(2) × 10^{-5} μs K^{-1}, b = 3.8(6) × 10^{-8} μs K^{-n}, n = 3.0(3).

Experimental Details

General remarks. TiOPc and VOPc were purchased from Sigma-Aldrich. The structural phase of TiOPc was declared as Type IV with > 99% purity degree. The structural phase of VOPc was not declared but it was identified by powder X-ray diffraction analysis as Type II by comparison with the simulated pattern generated from atomic coordinates obtained from single crystal X-ray diffraction data.[1]

Samples Preparation

Pure compounds

Diamagnetic Matrix: TiOPc, Type II. TiOPc, Type IV, (50 mg) was dissolved in 5 mL of a mixture of CF_3COOH (1 mL) and CH_2Cl_2 (4 mL). The green solution was stirred at room temperature for 10 minutes than poured into 50 mL of *iso*-propanol under stirring. The blue precipitate of TiOPc-II obtained was kept under stirring for 15 minutes and separated from the solution by centrifugation. The solid washed several times with *iso*-propanol and dried in oven at 80 °C for 2 hours. Yield: Quantitative.

***Paramagnetic Sample: VOPc, Type II* (1).** This compound was purified according to the procedure reported above for TiOPc-II, by filtering off the undissolved solid found in the CF_3COOH:CH_2Cl_2 green solution before pouring it in the precipitating solvent. Yield: 84%.

Doped Materials

***VOPc:TiOPc 1:10, Type II, VOPc$_{1:10}$-II* (2). 1** (18 mg, 3.12×10^{-2} mmol) and TiOPc-IV, (180 mg, 3.12×10^{-1} mmol) were dissolved in 20 mL of a mixture of CF_3COOH (4 mL) and CH_2Cl_2 (16 mL). The green solution was stirred at room temperature for 10 minutes than poured into 200 mL of *iso*-propanol under stirring. The blue precipitate of $VOPc_{1:10}$-II obtained was kept under stirring for 15 minutes and separated from the solution by centrifugation. The solid washed several times with *iso*-propanol and dried in oven at 80 °C for 2 hours. Yield: Quantitative.

***VOPc:TiOPc, 1:1000, Type II, VOPc$_{1:1000}$-II* (3).** This sample was prepared according to the procedure reported above for **2** by dissolving **1** (0.5 mg, 8.63×10^{-4} mmol) and TiOPc-IV, (497 mg, 8.63×10^{-1} mmol) in 55 mL of a mixture of CF_3COOH (11 mL) and CH_2Cl_2 (44 mL), and pouring the resulting green solution into 500 mL of *iso*-propanol. Yield: Quantitative.

Powder X-Ray Crystallography. Wide-Angle Powder X-Ray Diffraction (PXRD) patterns on polycrystalline samples were recorded on a *Bruker New D8 Advance DAVINCI* diffractometer in a theta-theta configuration equipped with a linear detector. The scans were collected within the range 5–35° (2θ) using CuK_α radiation (λ = 1.540 Å). The simulated patterns were generated from the atomic coordinates of the single-crystal structure solutions using the Mercury CSD 3.3 program[2] (copyright CCDC, http://www.ccdc.cam.ac.uk/mercury/) using a FWHM (full width at half maximum) of 0.60 and a 2θ step of 0.02.

Electron Paramagnetic Resonance. CW X-Band EPR spectra of all samples were recorded on a *Bruker Elexsys E500* spectrometer equipped with a SHQ cavity (ν = 9.47 GHz). Low temperature measurements were obtained using an *Oxford Instruments ESR900* continuous flow helium cryostat. The estimation of the relative abundance of the $TiOPc^{\cdot-}$ radical signal in TiOPc-II as received from Sigma-Aldrich and in **3** was obtained by double integration of the corresponding 300 K spectra - measured using the same instrumental parameters- of weighted

amount of samples. Pulsed EPR measurements were carried out with a *Bruker Elexsys E580* at X-band ($\nu \cong 9.70$ GHz) equipped with a flexline dielectric ring ENDOR resonator (*Bruker EN 4118X-MD4*). Temperatures between 4 and 250 K were obtained with *an Oxford Instruments CF935* continuous flow helium cryostat. Typical pulse lengths were 20 ns ($\pi/2$) and 40 ns (π). For Echo detected field swept EPR spectra, the Hahn Echo pulse sequence ($\pi/2$—τ — π —τ —echo) with fixed interpulse delay time τ = 200 ns, was applied while sweeping the magnetic field. Phase memory times measurements were obtained by measuring the primary echo decay with varying interpulse delay (τ) starting from τ = 98 ns at a fixed magnetic field. Spin–lattice-relaxation times were measured using the standard inversion recovery sequence (π — t_d — $\pi/2$—τ — π —τ— echo), with $\pi/2$ = 16 ns. Nutation measurements were performed with a nutation pulse (t_p) of variable length followed by a Hahn echo sequence (t_p-t_d— $\pi/2$—τ — π —τ—echo) with $t_d >> T_m$ (*i.e.* t_d = 7 μs for 4 K and 2 μs for RT measurements). The interpulse delay τ was 200 ns and the pulse length of the detection sequence was adjusted depending on the attenuation level of B_1.

Magnetic measurements. Alternate current (AC) susceptibility measurements were performed in the temperature range 1.8–40 K with applied magnetic fields up to 9 T on polycrystalline samples of compounds **1** (27.93 mg) and **2** (100.88 mg), by using a *Quantum Design Physical Property Measurement System (PPMS)* equipped with a AC susceptometer operating in the 10 Hz–10 kHz frequency range. Susceptibility data were corrected for the sample holder previously measured using the same conditions and for the diamagnetic contributions as deduced by using Pascal's constant tables.[3]

References

1. R. F. Ziolo, C. H. Griffiths and J. M. Troup, *J. Chem. Soc., Dalton Trans.*, **1980**, 2300–2302;
2. C. F. Macrae, P. R. Edgington, P. McCabe, E. Pidcock, G. P. Shields, R. Taylor, M. Towler and J. van de Streek, *J. Appl. Crystallogr.*, **2006**, *39*, 453−457;
3. G. A. Bain and J. F. Berry, *J. Chem. Educ.*, **2008**, *85*, 532–536.